Original Article

Fabrication and Characterization of Covalently Functionalized poly Caprolactone Scaffold for Bone Tissue Engineering Application

Negar Sadeghzade[1], Mahdi Nouri[1], Ali Shams Nateria[1], Masoud Soleimani[2,3*]

[1] Textile Engineering Department, University of Guilan, PO Box: 41635-3756 Rasht, Iran
[2] Hematology Department Faculty of Medicine, Tarbiat Modares University, Tehran, Iran
[3] Stem Cell Technology Research Center, Tehran, Iran

Abstract

Background: Healing bone involves osteoconductive and osteoinductive components as well as a scaffold with adequate porosity to allow good cell infiltration.

Materials and Methods: Herein, cytocompatibility and osteogenic induction potential of polycaprolactone (PCL) nanofibrous electrospun scaffold with different electron microscopy, MTT assay, DAPI and alizarin porosities (35%-90%) and chemical bonding was assessed through scanning red S staining, calcium content and alkaline phosphatase assay. Moreover, the relative expression of three important osteogenic-related genes *Col I, RUNX 2* and *osteocalcin* was studied.

Results: Covalent bonding played a more significant osteogenic role in scaffolds in scaffolds with lower porosity, namely H35cov. Although low porosity limits cell infiltration, substrate with lower porosities were easier to handle. On the other hand, substrates with higher porosity showed higher levels of cell proliferation, mineralization as well as osteogenic differentiation.

Conclusion: Results indicated that PCL scaffold with higher porosity degree up to 90%, covalently functionalized by collagen, and hydroxyapatite nanoparticles was a good candidate for bone tissue engineering applications.

Keywords: Fibrous scaffold, Osteogenic differentiation, Mesenchymal stem cells, Bone tissue engineering

*Corresponding Author: Masoud Soleimani, Hematology Department Faculty of Medicine, Tarbiat Modares University, Tehran, Iran, Tel: (+98) 912 1363881; E-mail: flute369@yahoo.com

Introduction

Several methods have been used to fabricate 3D porous scaffolds to mimic extra cellular matrix, including salt-leaching, freeze-drying, phase separation, self-assembly and gas forming However, the majority of these scaffolds fabricated do not sufficiently mimic the structure and function of bone ECM[1,2].

Electrospinning as a widely used method to design and fabricate scaffolds biomimicing the structure of ECM[2], has been considered as the most reliable and affordable method to fabricate continuous fibrous structures. Characteristics such as high surface area to volume ratio, high porosity and highly interconnected pores made electro-spun structures particularly conducive to cellular adhesion and growth. A wide range of natural polymers have been successfully electro-spun into fibrous scaffolds, however biodegradable and biocompatible synthetic polymers are preferred to be used as scaffolding materials due to their higher processing potential, mechanical strength and reproducible mechanical-chemical properties[3]. On the other hand, fabricating hybrid nanofibrous

substrates has also gained widespread interest by taking advantages of the biological property of the natural polymer and the mechanical property of the synthetic polymer[4]. Nevertheless, electro-spun scaffolds regularly show tightly packed layers of nanofibers with dense morphologies and limited pore sizes, which limits the nanofibrous structure to a simple 2D surface scaffold. Such nanostructure inhibits cell infiltration and growth through the substrate[2]. The pore sizes of the scaffolds need to supply cells with sufficient mechanical strength for significant stability and space as well as the delivery of nutrients and oxygen to the seeded cells within the scaffold to regenerate tissue[5].

Numerous approaches with some degree of favorable result to overcoming the inadequate porosity of electro-spun nanolayers have been studied. These methods include; fabrication of micro-nano structured porous scaffolds[6-10]. variation in electrospinning parameters[11-17], wet electrospinning[17-19], combining electrospinning with cell spraying[20], porogens incorporation[21-24], increasing fiber diameter[11,25,26].

Polycaprolactone (PCL) is one of the most frequently utilized; bioresorbable FDA approved synthetic biopolymers in tissue engineering scaffolding fields for its better processing and mechanical features as well as biocompatibility. However PCL shows a variety of drawbacks, such as intrinsic hydrophobic nature, poor interaction with the biological fluids, deficient cell adhesion and subsequent proliferation[3,4]. Concerning the morphology and structure of the substrate, biomimetic scaffolds must be tailored having high porosity and interconnected pores of several hundreds of microns, facilitating cell colonization and de-novo ECM biosynthesis. Nevertheless, in biological tissues, the ECM is furthermore composed of a complex merging network of protein fibers, mostly collagen and elastin, ranging from 10 to several hundreds of nanometers. Surface modification as a clear and practical approach is used to enhance the biocompatibility of the substrates[27]. Both collagen (Col-1) and hydroxyapatite (HA) have earned merit as bone regenerating scaffolds through their excellent biocompatibility with hard tissues, high osteoconductivity, osteoinductivity supplying osteogenic cells with reservoir of calcium and phosphate ions[28].

A novel perspective to medicate bone defects requires using osteoconductive and osteoinductive biocompatible materials containing bioactive modules to boost cell migration and cell transplantation[29].

To the best of our knowledge, very few studies have reported about fabricating an electrospun scaffold which has the advantages of porosity and combination of organic and inorganic component. In this study, we electrospun a nanofibrous scaffold which benefits both the interconnected porosity and presence of collagen type 1 and HA nanoparticles. Furthermore, the biological and mechanical assessments were carried out.

Methods

Electrospinning: Three types of fibrous scaffolds were prepared by electrospinning as is briefly described here: a solution of 12wt% PCL (M_w 80 KDa,Sigma) and 10wt% poly ethylene oxide (M_v 400,000 KDa, Sigam) and was prepared by adding the polymer palettes to a mixture of dimethylformamide and chloroform at a ratio of 2:8 and ethanol 90% (v/v) (Merck) respectively. The solution was loaded to a disposable syringe into a disposable syringe. Electrospinning was carried out for 8 hours by using a voltage of 24 KV, at a flow rate of 0.5 mL/h and working distance of 22 cm. PEO electrospinning was carried out using a voltage of 13 KV, working distance of 22 cm and at flow rate of 0.27 ml/h and 4.5 ml/h for scaffolds with 35% and 90% of porosity respectively. To introduce carboxyl groups on PCL, scaffolds were plasma treated. Later on, sacrificial fibers were removed by immersing in ethanol 90% for 3 days.

Total porosity was calculated by using the fallowing equations[30-34].

(1) $\text{Porosity} = (1 - \frac{\text{Nanofiber mat apparent density}}{\text{Bulk density of scaffold}}) \times 100$

(2) $\text{Nanofiber mat apparent density} = (\frac{\text{Nanofiber mat mass}}{\text{Nanofiber mat thickness} \times \text{Nanofiber mat area}})$

Grafting electro-spun scaffolds: Hydroxyapatite nanoparticles (nHA, 200 nm particle size, ≥97 Percentage, synthetic, Sigma) and collagen type 1(Bovine PureCol®,) were covalently bonded to hybrid PCL/PEO electrospun scaffolds. Procedure was carried out through the following steps: Electrospun scaffolds were incubated for 1 hour in water soluble carbodiimide

(2.5mg/ml) which was prepared by solving N-hydroxysuccinimide (NHS) and 1-ethyl-3-(3-dimethyaminopropyl) carbodiimide hydrochloride (EDC) in 2-morpholinoethanesulfonic acid monohydrate buffer(MES). Amine group was introduced to nHA using the coupling agent 3-aminopropeyl triethoxysilane (APTES). nHA immersed in APTES-distilled water (dw) solution (1:9) and kept at 95°C for 2 hours. nHA was added to electrospun scaffolds and kept for 1 hour at 4°C. Scaffolds were rinsed thoroughly, and incubated with EDC/NHS solution in MES buffer for another 2 hours at 4°C. Then samples were washed with dw and incubated overnight in Col I solution. Collagen solution (1.5 mg/mL) was prepared by diluting the PureCol® collagen solution in MES buffer. Scaffolds were then washed 8 times and each time for 5 minutes with phosphate buffer saline to remove any noncovalent bonded collagen. Substrates, which are described as H35phy and H90phy, were not treated by EDC/NHS.

SEM visualization and EDS mapping were used to characterize the nHA-grafted scaffolds. To evaluate collagen type 1 grafted via two different methods (just physical adsorption or by covalent boding), scaffolds were stained with trichrome. Collagen fibers were stained blue.

Cell culture studies: Human bone marrow-derived mesenchymal stem cells (hMSCs), (kindly donated from Stem Cell Technology Research Center), were cultured in high glucose growth medium (DMEM,Gibco) supplemented with 10% fetal bovine serum (FBS,Gibco), 1% fungizone and 1% penicillin/streptomycin (Gibco) in a humidified atmosphere with 5% CO_2 at 37°C. All cells were used before passage 4 for all the experiments.

The Scaffolds were sterilized using filtered 70% ethanol and seeded at a density of 15×10^3 cells /cm². After 48 h, normal medium was replaced with osteoinductive medium, which was prepared according to the protocol containing 10 mM β-glycerophosphate (Merck), 50 mg/mL L-ascorbic acid 2-phosphate (Sigma) and 10^{-8} M dexamethasone (Sigma).

The cell proliferation on the scaffolds was examined by using the colorimetric MTT assay which is based on the mitochondrial conversion of MTT (3-(4, 5-dimethylthiazol-2-yl)-diphenytetrazolim bromide to purple formazan crystals. After culturing the cells for a period of 1, 3, 7, 14 and 21 days the assay was performed in triplicate. Samples were incubated with MTT solution for 4 hours. Dimethyl sulfoxide was added to dissolve the formazan crystals. Absorbance was read at 570nm using an ELISA reader.

To evaluate cell proliferation on scaffolds using a fluorescent method, they were stained with 4', 6-diamidino-2-phenylindole on 1st, 14th and 21st days after cell seeding. Cells were then imaged using a fluorescent microscope.

Morphology of the samples and the cell attachment were evaluated at 1, 14 and 21 days of culture by scanning electron microscopy (SEM). The SEM images were captured using an accelerating voltage of 25 kV and working distance of 13.

Alizarin red staining: Alizarin Red-S is a dye that is able to bind to calcium salts selectively and the staining assay were performed to determine matrix maturation and mineralization. At day 21 of culture, scaffolds were washed twice with PBS and fixed with paraformaldehyde for 25 minutes at 4°C and 5 minutes at room temperature. The fixed samples were stained with 2% Alizarin red S (Sigma) for 5–10 min at room temperature. Finally, the cells were washed again with PBS for three times and depicted by inverted light microscope.

Table 1: Primers list of osteogenic markers.

Gene	Primer sequence
Collagen type I	F: 5′- TGCTTGAATGTGCTGATGACAGGG -3′
	R: 5′-TCCCCTCACCCTCCCAGTAT-3′
RUNX2	F: 5- CTGAGGTAACTTGCTAACG -3′
	R: 5'-ATCAATACACTAAGAAATGTTTCAAGG -3′
Osteocalcin	F: 5′- CTCTGCCTTAAACACACATTG -3′
	R: 5′- TTCCCTTTGCCCACCTC -3′

Alkaline phosphatase assay: As an early marker of osteogenesis of stem cells, ALP is an assessment of interest. Briefly, the method utilizes p-nitrophenyl phosphate (pNPP) that is converted by ALP to an equal amount of colored p-nitrophenol (pNP), a soluble yellow end-product measurable at 405 nm 27. At day, 1, 7, 14 and 21 the assay was carried according to Pars Azmun ALP kit. The experiment was carried out in triplicate and the results were normalized using micro Bicinchonic acid (BCA) protein assay kit (Pierce BCA: Thermo Scientific) fallowing the manufacturer's protocol.

Calcium content: At day 1, 7, 14 and 21 scaffolds were washed with PBS and transferred to microtubes.1 ml of HCL 0.6 N was added to each microtube. Reagents were mixed in accordance with Pars Azmun Calcium (CPC) kit instruction and absorbance was read using an ELISA reader at 570nm. The experiment was carried out in triplicate.

Real-Time PCR analysis: hMSCs were seeded on 7 different substrates: TCPS, Plasma treated PCL, H35 physical, H35 covalent, H90 physical and H90 covalent. After 7 and 14 days of osteogenic differentiation, total RNA was isolated according to the manufacturer's protocol (Fermentas, Thermo Fisher Scientific). RNA concentration was determined by absorbance at 260 nm, where an equivalent amount per of RNA (0.5 μg/group) was reverse transcribed into cDNA. Real-time PCR assays were performed by ABI sequence detection system (Applied Biosystems, Foster City, CA, USA). The primers for Runt related transcription factor 2 (*RUNX 2*), *osteocalcin* and Collagen type I (*Col I*) were synthesized by Fermentas. The results reported are representative of three independent experiments. Bone specific primers are listed in Table 1.

Statistical analysis and image processing: To verify whether the detected differences between the study groups were statistically significant, a two-tailed homoscedastic t-test was applied A value of $p < 0.05$ was considered to be statistically significant, while $0.05 < p < 0.10$ was regarded as a non-significant, but clear trend in cell or tissue response. Values are reported as the mean ± one standard deviation.

Results

Morphology and structure of the scaffolds: As it was mentioned earlier, Col I and nHA were incorporated to the scaffold via two methods; by physical adsorption and covalent bonds, which were through using EDC/NHS and APTES as coupling agents. To verify the presence of nHA and Col I and to show how effectively they were grafted via covalent bonding, SEM images and their corresponding EDX mapping images for calcium and phosphor as well as trichrome
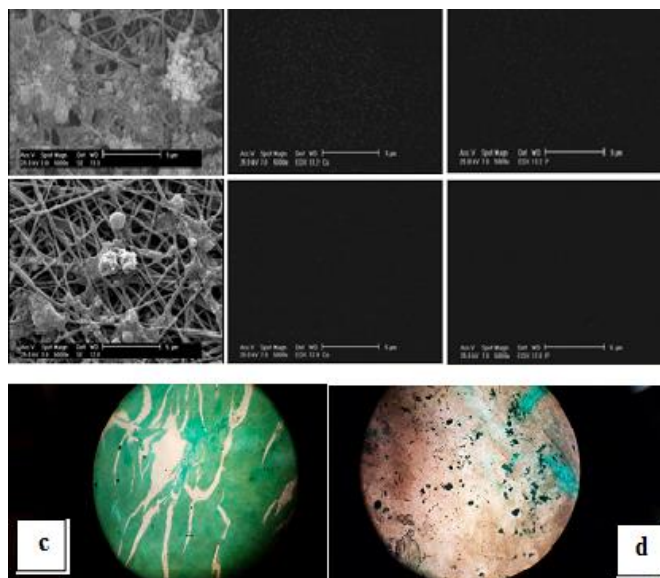
Figure 1. Selected SEM images and their corresponding EDX mapping images of nanofibrous scaffolds;(a) covalently nHA grafted PCL scaffold and (b) physically nHA adsorbed PCL scaffold, (c) covalently Col I grafted PCL and (d) physically Col I adsorbed PCL scaffold.
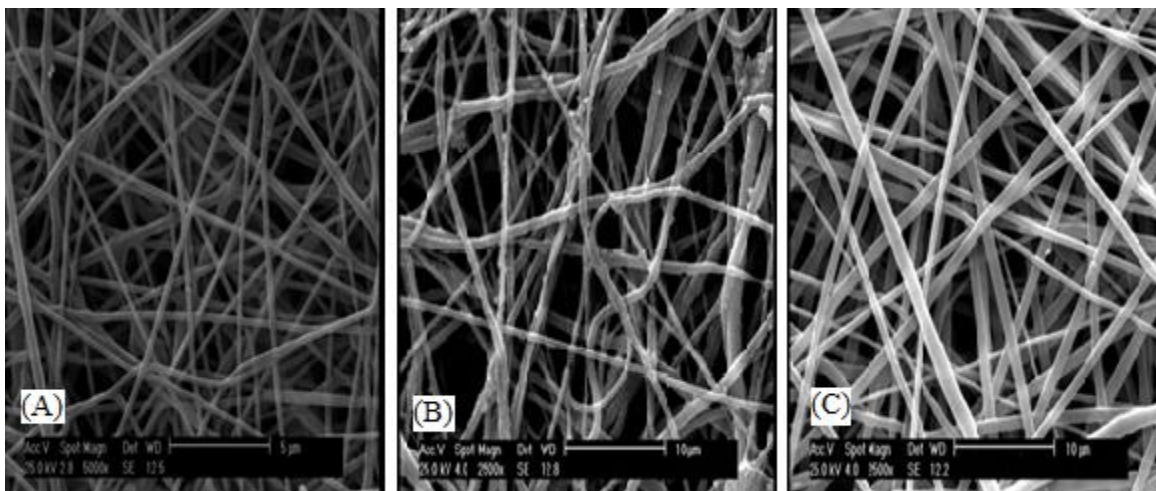
Figure 2. SEM images of the scaffolds; (A) Electrospun random PCL nanofibers, (B) 90% Hybrid electrospun scaffold, (C) 35% Hybrid electrospun scaffold.
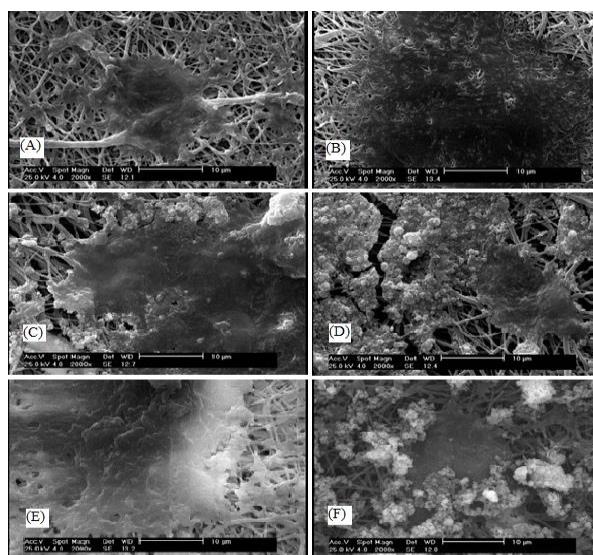
Figure 3. SEM images of the scaffolds after 14 days of cell culture. A) PCL, B) Covalent PCL scaffold, C) H35physical, D) H35Cov, E) H90 Physical, F) H90 Covalent.
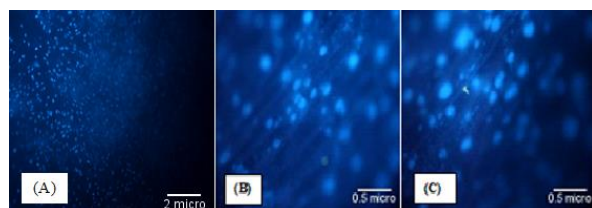
Figure 4. Fluorescent microscopy images of the scaffolds. A) PCL B) H90Physical   C) H90 Covalent.

staining were used. SEM images and the corresponding EDX mapping show the homogenous distribution of HA nanoparticles on the surface of the electrospun scaffold, which was grafted by using the coupling agents. Trichrome staining showed more Col I stained area on covalently bonded structures (Figure 1).

Characterization of fibers and scaffolds: Since the structure and morphology of the electrospun scaffolds plays an important role in stem cells fate, it was studied thoroughly via SEM images as are shown in figure 2. Image (A) shows the PCL plasma treated scaffold with the average fiber diameter of 250 ± 7 nm ranging from 150 to 550 nm and average pore size of 350 nm^2. Figure 2 also shows the micrograph images of H90 and H35, which are they hybrid scaffolds with 90% and 35% of PEO fibers served as sacrificial fibers. In H90 scaffolds, average fiber diameter was estimated to be 500 ± 15 nm with diameter ranging from 200-700 nm and average pore size of $7\mu^2$ (figure 2B). In figure 2C electrospun PCL scaffold is showed with average fiber diameter of 700 ± 20 nm ranging from 200 to 1200 nm and average pore size of $1.8\mu^2$.

Figure 3 shows the SEM image of cells- nanofibrous scaffolds interaction after 14 days. Image 3A shows PCL scaffold in which cells seemed to be poorly attached. Image 3B shows PCL scaffold with covalently bonded nHA and Col I (PCL covalent), showed better cell spreading. Image 3C is the hybrid scaffold with 35% of porosity which nHA and Col I were just physically adsorbed on the scaffolds (H35physical). Better cell adhesion and mineral compounds could be observed. Image 3D is the hybrid scaffold with 35% porosity that nHA and Col I were covalently bonded to the fibrous structure using appropriate coupling agents (H35Covalent). More nano particles could be seen on the scaffold. Image 3E is the hybrid scaffold with 90%
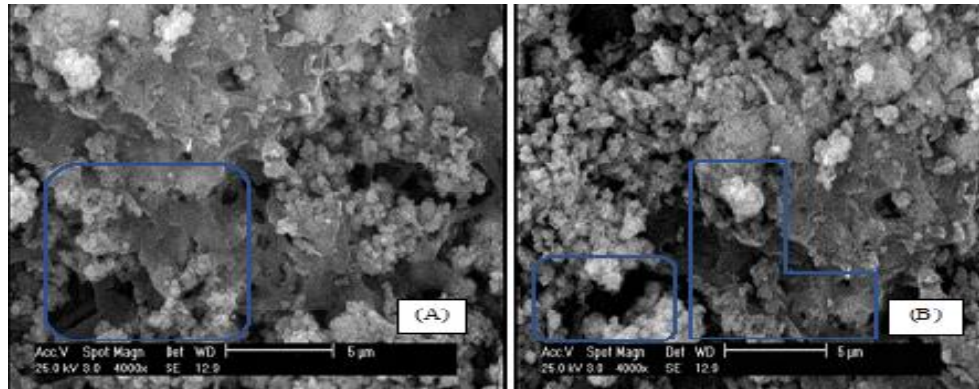
Figure 5. SEM Images of scaffolds with 90% porosity. Signs of cell infiltrations are marked.
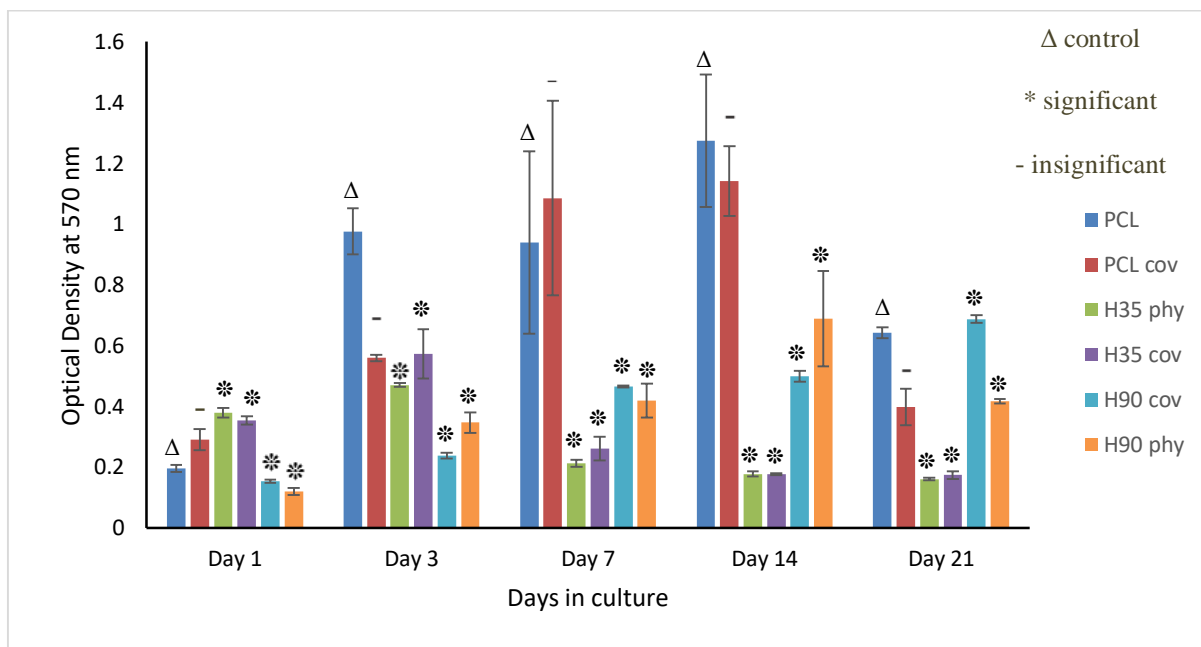
Figure 6. Proliferation MSCs on different scaffolds. The results given are representative of three independent experiments.

porosity nHA and Col I were just physically adsorbed on the scaffolds (H90 Physical). Better cell attachment and spreading was seen. Image 3F is the scaffold with 90% porosity and covalently bonded nHA and Col I 1(H90 covalent). More nano particles remained attached to the scaffold through rinsing and cell culture media changes.

Fluorescent microscopy analysis was used to confirm the cell attachment on scaffolds. Figure 4 shows the scaffolds after 14 days of cell culture. Cells were attached well enough on the scaffolds to stand the stresses. Cells in both control (PCL scaffolds) and functionalized scaffolds were found to exhibit good spreading and proliferation.

In vitro studies:

Cytotoxicity test: The MTT assay, as a rapid and standardized way to determine cells viability and material contains significant quantities of biological harmful extract was used to evaluate the cell viability and proliferation on the fibrous scaffolds. Figure 6 shows the MTT results of the samples. PCL scaffold was considered as the control sample (Δ) and the scaffold with tailored porosity and modified surface were studied as test samples. No cytotoxicity was observed. All scaffolds showed increase in number of cells up to day 14 and then a decrease was observed. Average cell number is at its highest on day 14.

Alizarin red S staining: The assay was used to stain the
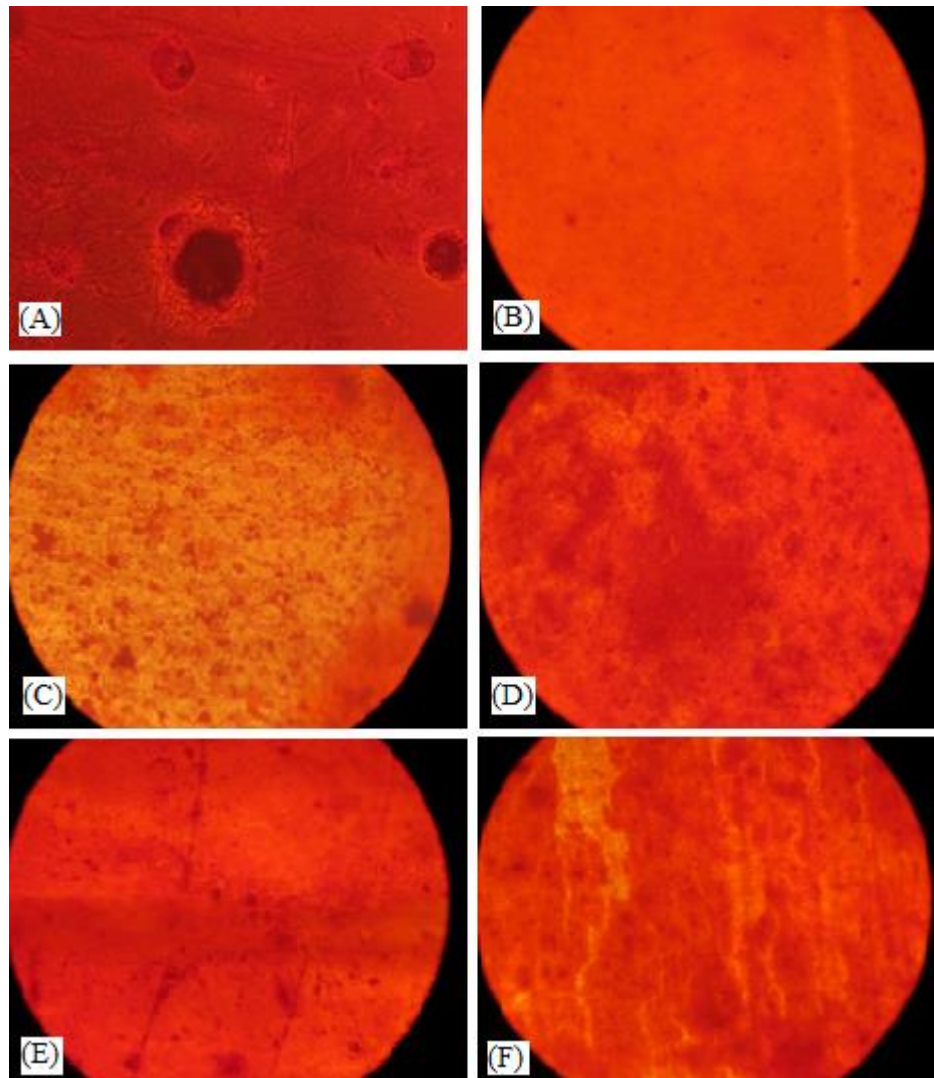
Figure 7. Photomicrographs of alizarin red staining of calcium deposition A) tissue culture polystyrene, B) Plasma treated PCL, C) H35 physical, D) H35 covalent, E) H90 physical, F) H90 covalent after 21 days of osteogenic differentiation.

intracellular Ca as well as the Ca-binding proteins and proteoglycans in a chelating process[35]. Figure 7 depicts images of the alizarin red stained scaffolds after 21 days of cell culture. Darker areas represent alizarin red staining which means mesenchymal stem cells were able to differentiate into osteogenic lineage and mineralize. Image (A) shows cells on TCPS. The image shows that there is just one main mineralized region almost in the center of well and some spots around. Image (B), shows PCL scaffold. Mineralized areas are formed like small and scattered spots almost all over the scaffold. In image (C) H35 physical, mineralized areas were still formed in dot like shapes. In image (D) H35 covalent, mineralized regions are formed in bigger zones. In Image (E) H90 physical,

calcium deposition was in few thick lines across the scaffold. Image (F), which represents H90 covalent, calcium containing regions were large enough that were able to integrate and represent connected areas of differentiated cells. The differentiation of MSCs into osteoblasts is associated with mineralization leading to the deposition of calcium in cytoplasm[37].

Calcium content: To measure ECM calcium deposits for bone nodule formation, the accumulated Ca in the secreted ECM of the osteoblasts as well as Ca-binding proteins and proteoglycans was quantified using the Ca content kit and reported in figure 8.

TCPS results indicated that Ca content increased continuously during 21 days of differentiation. PCL scaffold decreased in the first 7 days of the culturing
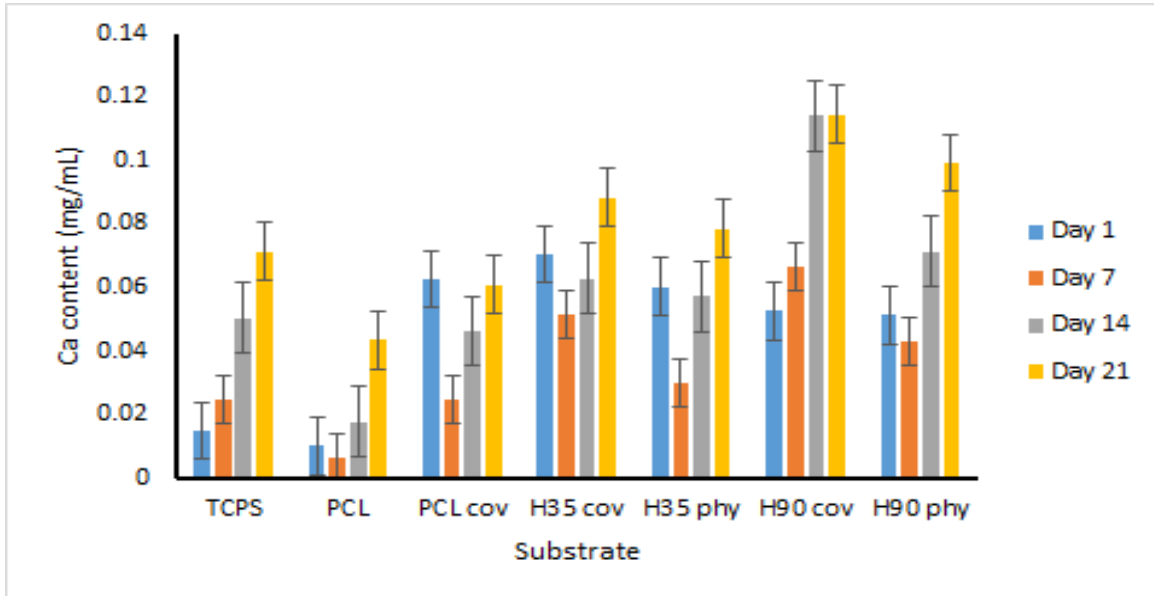
Figure 8. Ca content of the substrates of bone marrow mesenchymal stem cells, on 1st, 7th, 14th and 21st day of osteogenic differentiation. The results given are representative of three independent experiments. (considering TCPS as the control, the change in Ca content of all the scaffolds were insignificant, p≤0.05).
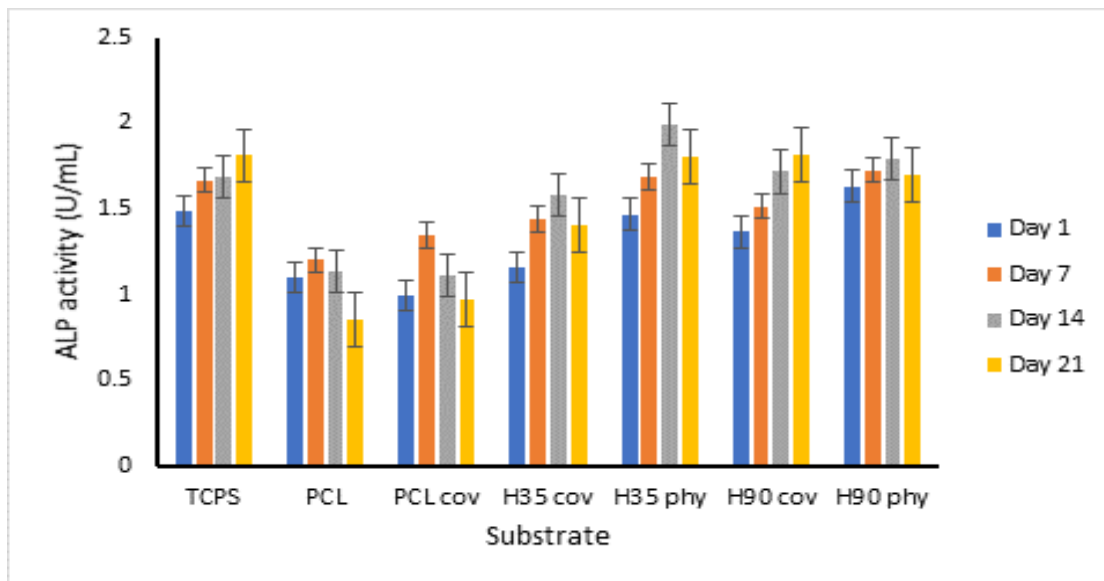
Figure 9. Alkaline phosphatase (ALP) activity of bone marrow mesenchymal stem cells, on 1st,7th, 14th and 21st day, during osteogenic differentiation. The results given are representative of three independent experiments. (considering TCPS as the control, the change in ALP activity of all scaffolds except H90cov and H90phy where significant, p≤0.05).

period but increased from day 7 to day 21. PCL covalent showed the same trend as PCL but the Ca content values were higher. Sample 4, H35 covalent also showed the same trend during the 21-day cell culture but the amount of Ca was higher than the 3 previous samples. Ca content of H35 physical also fallowed the same pattern as the earlier mentioned scaffolds. However, H90 covalent showed a different

tendency. Total calcium content increased from day 1 to day 14 of the culture then the values seemed to reach a plateau. The scaffold had the highest Ca content values. H90 physical showed the same trend as the first 4 above scaffolds. Although the numbers were higher. **Alkaline phosphatase assay:** ALP secretion as an early-stage marker of osteogenic differentiation was regarded as a critical test among the various biological
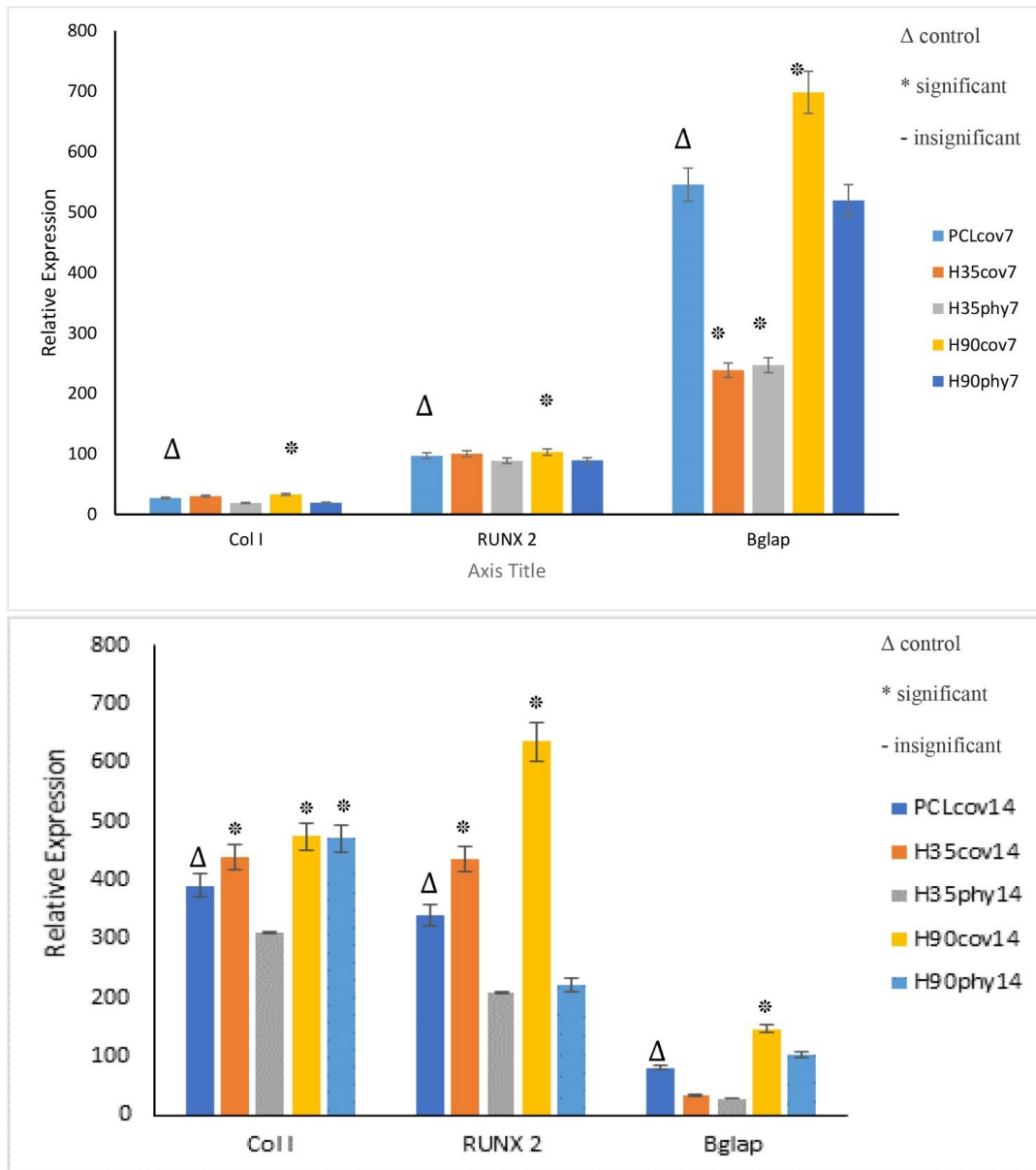
Figure 10. Relative expression of *Col I, RUNX 2* **(Runt-related transcription factor 2) and** *Osteocalcin* **(bone gamma-carboxyglutamic acid containing protein) of bone marrow mesenchymal stem cells, on 7th and 14th day, during osteogenic differentiation. The results given are representative of three independent experiments (Changes in osteogenic gene expression on day 7th and 14th of the scaffolds were significant, p≤0.05).**

assays to estimate the activity rate of osteoblasts in the scaffolds[36].

As figure 9 shows, cells on TCPS showed an increasing tendency during the induction time. Sample 2, PCL as well as sample 3, PCL covalent showed an increase of ALP activity from day 1 to 7, then a decrease until the end of differentiation period. The trend changed as ALP activity of H35 covalent, H35 physical and H90 physical were studied. The increase

in ALP activity continued to 14th day of the assay and then the activity decreased. As cells on H90 covalent were studied, results indicated that ALP actvity increased continuously during 21 days of differentiation.

Real-Time polymerase chain reaction: To investigate the effects of chemical and physical structure of the scaffolds on osteogenesis process, the relative expression of four important osteogenic related genes

was studied at 7 and 14 days after cell seeding. The RT-PCR results showed that osteogenic related genes were detected in the culture system. The levels of gene expression (quantified by relative expression using the housekeeping gene *β2M* as a control) in the scaffolds after 7 and 14 days of culture are shown in figure 10. At day 7 no sample had a high expressiong of *Col I* but it upregulated at day 14. The expression of *RUNX 2* also increased at day 7 and 14, only in H35 physical, it showed lower levels of expression at day 14. All samples showed higher levels of *Osteocalcin* expression at day 7 than day 14 of the differentiation period.

Discussion

SEM images as well as EDX mapping verified successful formation of covalent bonds between nanofibers and HA nanoparticles which would hopefully work in the benefit of better cell recognition and differentiation during the cell culture period. Since nanofibers provided nanoparticles with bonding sites –activated carboxyl groups- they had the opportunity to penetrate into the scaffold (Figure 1.a), as better infiltration is one of the main aim of this study. nHA which were physically adsorbed to the scaffold couldn't last through the washing process (Figure 1.b) and the poorly attached residual nanoparticles would be washed away during the cell culture period. Therefore, they cannot be a suitable and supporting substrate for cellular demands. The same trend was observed for trichrome stained scaffolds.

Figure 2 image (A) showed a dense scaffold of beadless fibers with smooth surface and no merging on cross sections, which would later prevent cellular infiltration. Morphological characteristics of scaffolds will be studied thoroughly in further papers. As porosity of PCL scaffold was analyzed in a recently published study[37].

Cells poorly attached to the surface of the dense structure of PCL scaffold, which showed no sign of cell, infiltrate due to small pores. PCL covalent showed better cell attachment and spreading because of the minerals and biomolecules on the surface, which supply cells with bioactive sites. H35 covalent, had better cell interaction due to nHA and Col I and improved porosity. However, no cell infiltration was

observed. On H35 physical and H90 covalent, nHA was mainly washed away during rinsing process or changing the cell culture media. nHA and Col I could stand the rinsing and changing media on H90 covalent helping the sample with better cell attachment and spreading. Tailoring the porosity was effective, since better cell infiltration was observed on image E and F.

Images of the DAPI stained scaffolds were as an indicative of biocompatible environment of the samples[38]. This may also be due to Col I and calcium present in the composition which played a critical role in mediating the better cell proliferation[52,53]. In scaffolds with 90% of porosity, cells not only adhered to the surface of the fibrous nanolayer but also were able to infiltrate through the network of nanofibers. In these scaffolds, photos could not be taken with all the cells in good clarity. That is because cells were not just on the surface of the scaffolds. This was not observed in other scaffolds with less porosity.

Since better cell infiltration was one of the main aim of this study, three groups of scaffolds were studied. PCL scaffolds had dense structure; further porosity was added to the scaffolds by using PEO fibers, as sacrificial fibers (35% more porosity comparing to PCL scaffolds) and the third group was PCL scaffolds with 90% porosity, which was provided by PEO, removed fibers. Only SEM images of the third group showed that cells were able to go through the pores and infiltrate into the fibrous scaffold (figure 5A-B).

Focusing on cell proliferation, the increase in cell number until 14th day of culture could be interpreted as rise in cell differentiation. Augmented differentiation after day 14 could be the beneficial effect of covalent bonding between biomolecules / minerals and nanofibrous structure, such as H90 covalent scaffold.

Since the decline in OD values after 14th day was interpreted as a sign of increase in osteogenic differentiation, higher porosity of the scaffolds and biological and mineral molecules engraftment to the substrates, were appropriate for both the cell proliferation and osteogenic differentiation. Figure 6 showed significant increase in cell number at 3, 7 and 14 days after cell culture. This may be due to collagen and calcium containing compound present in the composition, which played vital role in regulating the better cell proliferation. In addition, the proliferation might be mediated by activating the intercellular

proliferative mechanism in osteoblasts for reconstruction of the defective site of the bone[39].

As it was depicted in Figure 7, mineralized area in TCPS, was mainly limited to a circular region. Although TCPS is a very common substrate to culture cells, it has no resemblance to fibrillary structure of ECM. Although cell seeding efficiency is higher on TCPS and there is no risk of losing cells slipping into the sides-unlike seeding cells on electro-spun scaffold- it was not able to meet cellular needs structural and also component wise. This means, TCPS had no fibrous arrangement as it was earlier mentioned, and it could not supply MSCs with calcium reservoir nor any biological cues. Cells on such substrate can only proliferate in one dimension and after reaching a certain confluence they might detach from the plate and will not be able to form any 3D structure. Small and scattered alizarin red stained regions in image (B), which shows the PCL sample, means that mineralization was not limited to a few areas. However, mineralized area are so small that are more like scattered dots on the electro-spun scaffold. In image (C) mineralized areas are observed as small spots on the scaffold. Comparing to image (B), better mineralization could be due to presence of nHA and Col I, however PCL scaffold had dense structure, and the porosity percentage (35%) was not sufficient for cells. Bigger mineralized regions in image (D) confirmed that MSCs were able to differentiate to osteogenic cells and cover the scaffold more, comparing to previous samples. Covalently functionalized surface by biomolecules and minerals were able to enhance osteogenic differentiation. In image (E) with integrated areas of differentiated cells, thanks to higher porosity of the scaffold, cells were able to attach and proliferate better which means more cell contact that is an important parameter for successful cell differentiation with higher yield. Since cell differentiation is highly contact dependent it is very important that cells can spread efficiently on and through the nanofibrous structure. The structure in image E, supplied MSCs with an appropriate substrate, resembling tissue specific extracellular matrix in both structure and composition. Image (F) shows that cells were able to mineralize in smaller areas, and in spite of appropriate porosity of the scaffold, it was not able to perform as a suitable

substrate as sample (E).

Covalent bonding and functionalizing of the substrates worked together in the favor of cells attachment, proliferation and consequently differentiation. Figure 9, confirmed that the ALP activity of BMSCs increased with time throughout the test period. Since bone healing is a long process, this would be significantly one of the desired characteristics of H90cov scaffolds to be considered in bone tissue engineering[27].

The osteoblast differentiation and mineralization is reflected in the activation of osteoblast differentiation marker genes as well as depositions of calcium molecules, which promote the ECM formation. Covalently grafted col I/nHA and improved porosity of H90 covalent effectively enhanced bone differentiation and produced the highest level of osteocalcin on 7th day. Meanwhile, the highest expression of Col I and Runx2 was noted after 14 days of culture. The expression levels of major transcription factor for bone *Runx2*, differentiation marker genes *Col-I* and *osteocalcin* were upregulated in presence of osteogenic stimulant compared to absence of osteogenic stimulant[40-43]. RT-PCR data confirmed that osteogenic differentiation of BMSCs was superior in scaffolds with enhanced porosity as well as covalently containing osteoinductive collagen type I and osteoconductive nHA.

Conclusion

The regeneration of fractured bones by tissue engineering is hugely dependent on the application of stem cells in combination with bioactive scaffolds. Commitment of MSCs to a particular lineage depends on intracellular and extracellular cues to guide differentiation. The synergistic effects of enhanced scaffold porosity increase the adhesion, proliferation and infiltration of osteoblast cells on the scaffold and nHA. Scaffold has a crystalline structure similar to bone mineral phase and is considered as "gold-standard" for osteoconductive scaffolds, as well as collagen type I, which has direct impact on increased cell adhesion and ALP activity due to increased calcium deposits production and thus, increased matrix mineral level. Scaffolds with higher porosity showed higher rate of cellular proliferation and more stable trend of mineralization and ALP as the results of Ca content, MTT and ALP assay showed. Unlike physical bonded

Col I and nHA, covalently bonded Col I and nHA were able to contribute to osteogenic differentiation of MSCs until the end of culture period. This is a very important since bone healing is a relatively time consuming process. Scaffolds with higher porosity and covalent bonding with the biomolecules and biominerals showed higher expression of osteogenic genes. Covalent bonding also helped PCL scaffold to have a relatively higher gene expression in absent of sufficient porosity. As it was seen in *RUNX2* expression, covalent bonding played a more critical role in the scaffolds with lower porosities. The results ultimately helped to emerge osteogenesis of BMSCs and osteogenic differentiation and obtain the desired mineral matrix, confirming that the aforementioned nano fibrillar structure has the essential criteria to be considered in bone tissue engineering applications.

Acknowledgment

None.

References

1. Loh QL, Choong C. Three-dimensional scaffolds for tissue engineering applications: role of porosity and pore size. Tissue Eng B: Reviews 2013;19(6):485-502.

2. Hwang PT, Murdock K, Alexander GC, Salaam AD, Ng JI, Lim DJ, Dean D, Jun HW. Poly (ε-caprolactone)/gelatin composite electrospun scaffolds with porous crater-like structures for tissue engineering. J Biomed Mater Res A 2016 Apr;104(4):1017-29.

3. Li W, Hu Y, Shi L, Zhang X, Xiong L, Zhang W, Ullah I. Electrospinning of Polycaprolactone/Pluronic F127 dissolved in glacial acetic acid: fibrous scaffolds fabrication, characterization and in vitro evaluation. J Biomater Sci Polym Ed 2018 ;29(10):1155-67.

4. Yao Q, Cosme JG, Xu T, Miszuk JM, Picciani PH, Fong H, Sun H. Three dimensional electrospun PCL/PLA blend nanofibrous scaffolds with significantly improved stem cells osteogenic differentiation and cranial bone formation. Biomat 2017; 115:115-27.

5. Kim HY, Kim HN, Lee SJ, Song JE, Kwon SY, Chung JW, Lee D, Khang G. Effect of pore sizes of PLGA scaffolds on mechanical properties and cell behaviour for nucleus pulposus regeneration in vivo. J Tissue Eng Regen Med 2017 ;11(1):44-57.

6. Thorvaldsson A, Stenhamre H, Gatenholm P, Walkenström P. Electrospinning of highly porous scaffolds for cartilage regeneration. Biomacromolecules 2008 ;9(3):1044-9.

7. Soliman S, Pagliari S, Rinaldi A, Forte G, Fiaccavento R, Pagliari F, Franzese O, Minieri M, Di Nardo P, Licoccia S, Traversa E. Multiscale three-dimensional scaffolds for soft tissue engineering via multimodal electrospinning. Acta Biomat 2010 Apr 1;6(4):1227-37.

8. Kim GH, Park YD, Lee SY, El-Fiqi A, Kim JJ, Lee EJ, Kim HW, Kim EC. Odontogenic stimulation of human dental pulp cells with

bioactive nanocomposite fiber. J Biomater Appl 2015;29(6):854-66.

9. Huang Y, Wang J, Yang F, Shao Y, Zhang X, Dai K. Modification and evaluation of micro-nano structured porous bacterial cellulose scaffold for bone tissue engineering. Mater Sci Eng C Mater Biol Appl 2017; 75:1034.

10. Hwang CM, Sant S, Masaeli M, Kachouie NN, Zamanian B, Lee SH, Khademhosseini A. Fabrication of three-dimensional porous cell-laden hydrogel for tissue engineering. Biofabrication 2010;2(3):035003.

11. Pham QP, Sharma U, Mikos AG. Electrospinning of polymeric nanofibers for tissue engineering applications: a review. Tissue Eng 2006 ;12(5):1197-211.

12. Rnjak-Kovacina J, Wise SG, Li Z, Maitz PK, Young CJ, Wang Y, Weiss AS. Tailoring the porosity and pore size of electrospun synthetic human elastin scaffolds for dermal tissue engineering. Biomaterials 2011 ;32(28):6729-36.

13. Vaquette C, Cooper-White JJ. Increasing electrospun scaffold pore size with tailored collectors for improved cell penetration. Acta Biomat 2011 ;7(6):2544-57.

14. Blakeney BA, Tambralli A, Anderson JM, Andukuri A, Lim DJ, Dean DR, Jun HW. Cell infiltration and growth in a low density, uncompressed three-dimensional electrospun nanofibrous scaffold. Biomaterials 2011 ;32(6):1583-90.

15. Soliman S, Sant S, Nichol JW, Khabiry M, Traversa E, Khademhosseini A. Controlling the porosity of fibrous scaffolds by modulating the fiber diameter and packing density. J Biomed Mater Res B 2011 Mar 1;96(3):566-74.

16. Cai YZ, Zhang GR, Wang LL, Jiang YZ, Ouyang HW, Zou XH. Novel biodegradable three-dimensional macroporous scaffold using aligned electrospun nanofibrous yarns for bone tissue engineering. J Biomed Mater Res A 2012 ;100(5):1187-94.

17. Cai S, Xu H, Jiang Q, Yang Y. Novel 3D electrospun scaffolds with fibers oriented randomly and evenly in three dimensions to closely mimic the unique architectures of extracellular matrices in soft tissues: fabrication and mechanism study. Langmuir 2013 ;29(7):2311-8.

18. Ki CS, Lee KH, Baek DH, Hattori M, Um IC, Ihm DW, Park YH. Dissolution and wet spinning of silk fibroin using phosphoric acid/formic acid mixture solvent system. J Appl Polym Sci 2007 ;105(3):1605-10.

19. Heo J, Nam H, Hwang D, Cho SJ, Jung SY, Cho DW, Shim JH, Lim G. Enhanced cellular distribution and infiltration in a wet electrospun three-dimensional fibrous scaffold using eccentric rotation-based hydrodynamic conditions. Sens Actuators B Chem 2016; 226:357-63.

20. Stankus JJ, Guan J, Fujimoto K, Wagner WR. Micro integrating smooth muscle cells into a biodegradable, elastomeric fiber matrix. Biomaterials ;27(5):735-44.

21. Lee CH, Shin HJ, Cho IH, Kang YM, Kim IA, Park KD, Shin JW. Nanofiber alignment and direction of mechanical strain affect the ECM production of human ACL fibroblast. Biomaterials 2005 ;26(11):1261-70.

22. Wang P, Zhao L, Liu J, Weir MD, Zhou X, Xu HH. Bone tissue engineering via nanostructured calcium phosphate biomaterials and stem cells. Bone Res 2014; 2:14017.

23. Salerno A, Guarino V, Oliviero O, Ambrosio L, Domingo C. Bio-safe processing of polylactic-co-caprolactone and polylactic acid

blends to fabricate fibrous porous scaffolds for in vitro mesenchymal stem cells adhesion and proliferation. Mat Sci Eng C. 2016; 63:512-21.

24. Rnjak-Kovacina J, Weiss AS. Increasing the pore size of electrospun scaffolds. Tissue Eng B: Reviews 2011 ;17(5):365-72.

25. Sisson K, Zhang C, Farach-Carson MC, Chase DB, Rabolt JF. Fiber diameters control osteoblastic cell migration and differentiation in electrospun gelatin. J Biomed Mat Res A. 2010 ;94(4):1312-20.

26. Yu Y, Hua S, Yang M, Fu Z, Teng S, Niu K, Zhao Q, Yi C. Fabrication and characterization of electrospinning/3D printing bone tissue engineering scaffold. RSC Advances 2016;6(112):110557-65.

27. Yang C, Huan Z, Wang X, Wu C, Chang J. 3D printed Fe scaffolds with HA nanocoating for bone regeneration. ACS Bioma Sci Eng 2018 ;4(2):608-16.

28. Prosecká E, Rampichová M, Litvinec A, Tonar Z, Králíčková M, Vojtová L, Kochova P, Plencner M, Buzgo M, Míčková A, Jančář J. Collagen/hydroxyapatite scaffold enriched with polycaprolactone nanofibers, thrombocyte-rich solution and mesenchymal stem cells promotes regeneration in large bone defect in vivo. J Biomed Mat Res A. 2015 ;103(2):671-82.

29. Niu B, Li B, Gu Y, Shen X, Liu Y, Chen L. In vitro evaluation of electrospun silk fibroin/nano-hydroxyapatite/BMP-2 scaffolds for bone regeneration. J Biomater Sci Polym Ed 2017 ;28(3):257-70.

30. Gao Y, Shao W, Qian W, He J, Zhou Y, Qi K, Wang L, Cui S, Wang R. Biomineralized poly (l-lactic-co-glycolic acid)-tussah silk fibroin nanofiber fabric with hierarchical architecture as a scaffold for bone tissue engineering. Mat Sci Eng: C .2018 Mar 1; 84:195-207.

31. Song J, Kim J, Woo HM, Yoon B, Park H, Park C, Kang BJ. Repair of rabbit radial bone defects using bone morphogenetic protein-2 combined with 3D porous silk fibroin/β-tricalcium phosphate hybrid scaffolds. J Biomater Sci Polym Ed 2018 ;29(6):716-29.

32. Zhang K, Fan Y, Dunne N, Li X. Effect of microporosity on scaffolds for bone tissue engineering. Regen Biomater 2018 5;5(2):115-24.

33. Murphy WL, Dennis RG, Kileny JL, Mooney DJ. Salt fusion: an approach to improve pore interconnectivity within tissue engineering scaffolds. Tissue Eng 2002 ;8(1):43-52.

34. He W, Ma Z, Yong T, Teo WE, Ramakrishna S. Fabrication of collagen-coated biodegradable polymer nanofiber mesh and its potential for endothelial cells growth. Biomat 2005 ;26(36):7606-15.

35. Sadeghzade N, Nouri M, Nateri AS, Soleimani M. Studying the Nanofibrous Structure of Polycaprolactone Scaffold via Image Processing Technique. J Bionanoscience. 2018 Feb 1;12(1):76-86.

36. Wang K, Zhu M, Li T, Zheng W, Xu LL, Zhao Q, Kong D, Wang L. Improvement of cell infiltration in electrospun polycaprolactone scaffolds for the construction of vascular grafts. J Biomed Nanotechnol 2014 ;10(8):1588-98.

37. Kumar SD, Abudhahir KM, Selvamurugan N, Vimalraj S, Murugesan R, Srinivasan N, Moorthi A. Formulation and biological actions of nano-bioglass ceramic particles doped with Calcarea phosphorica for bone tissue engineering. Mater Sci Eng C 2018; 83:202-9.

38. Moorthi A, Vimalraj S, Avani C, He Z, Partridge NC, Selvamurugan N. Expression of microRNA-30c and its target genes in human osteoblastic cells by nano-bioglass ceramic-treatment. Int J Biol Macromol 2013; 56:181-5.

39. Niranjan R, Koushik C, Saravanan S, Moorthi A, Vairamani M, Selvamurugan N. A novel injectable temperature-sensitive zinc doped chitosan/β-glycerophosphate hydrogel for bone tissue engineering. Int J Biol Macromol 2013; 54:24-9.

40. Ghasemzadeh M, Hosseini E, Ahmadi M, Kamalizad M, Amirizadeh N. Comparable osteogenic capacity of mesenchymal stem or stromal cells derived from human amnion membrane and bone marrow. Cytotechnology. 2018;70(2):729-39.

41. Huang TY, Su WT, Chen PH. Comparing the Effects of Chitosan Scaffolds Containing Various Divalent Metal Phosphates on Osteogenic Differentiation of Stem Cells from Human Exfoliated Deciduous Teeth. Biol Trace Elem Res 2018 :1-1.

42. Moorthi A, Saravanan S, Srinivasan N, Partridge NC, Zhu J, Qin L, Selvamurugan N. Synthesis, characterization and biological action of nano-bioglass ceramic particles for bone formation. J Biomat Tissue Eng 2012 ;2(3):197-205.

43. Sahithi K, Swetha M, Prabaharan M, Moorthi A, Saranya N, Ramasamy K, Srinivasan N, Partridge NC, Selvamurugan N. Synthesis and characterization of nanoscalehydroxyapatite-copper for antimicrobial activity towards bone tissue engineering applications. J Biomed Nanotechnol 2010 ;6(4):333-9.